Environmental Pollution 221 (2017) 94–104

Contents lists available at ScienceDirect

Environmental Pollution

journal homepage: www.elsevier.com/locate/envpol

Impact of diurnal variability and meteorological factors on the $PM_{2.5}$ - AOD relationship: Implications for $PM_{2.5}$ remote sensing☆

Jianping Guo [a, *], Feng Xia [a], Yong Zhang [b, **], Huan Liu [a, e], Jing Li [c], Mengyun Lou [a, e], Jing He [a], Yan Yan [a], Fu Wang [d], Min Min [d], Panmao Zhai [a]

[a] State Key Laboratory of Severe Weather & Key Laboratory of Atmospheric Chemistry of CMA, Chinese Academy of Meteorological Sciences, Beijing 100081, China

[b] Meteorological Observation Center, China Meteorological Administration, Beijing, 100081, China

[c] Department of Atmospheric and Oceanic Sciences, Peking University, Beijing 100871, China

[d] National Satellite Meteorological Center, Beijing 100081, China

[e] College of Earth Sciences, University of Chinese Academy of Sciences, Beijing 100049, China

A R T I C L E I N F O

Article history:
Received 1 October 2016
Received in revised form
10 November 2016
Accepted 14 November 2016
Available online 23 November 2016

Keywords:
PM2.5
AOD
China
Correlation analysis
Cloud fraction
Relative humidity

A B S T R A C T

$PM_{2.5}$ retrieval from space is still challenging due to the elusive relationship between $PM_{2.5}$ and aerosol optical depth (AOD), which is further complicated by meteorological factors. In this work, we investigated the diurnal cycle of $PM_{2.5}$ in China, using ground-based PM measurements obtained at 226 sites of China Atmosphere Watch Network during the period of January 2013 to December 2015. Results showed that nearly half of the sites witnessed a $PM_{2.5}$ maximum in the morning, in contrast to the least frequent occurrence (5%) in the afternoon when strong solar radiation received at the surface results in rapid vertical diffusion of aerosols and thus lower mass concentration. $PM_{2.5}$ tends to peak equally in the morning and evening in North China Plain (NCP) with an amplitude of nearly twice or three times that in the Pearl River Delta (PRD), whereas the morning $PM_{2.5}$ peak dominates in Yangtze River Delta (YRD) with a magnitude lying between those of NCP and PRD. The gridded correlation maps reveal varying correlations around each $PM_{2.5}$ site, depending on the locations and seasons. Concerning the impact of aerosol diurnal variation on the correlation, the averaging schemes of $PM_{2.5}$ using 3-h, 5-h, and 24-h time windows tend to have larger *R* biases, compared with the scheme of 1-h time window, indicating diurnal variation of aerosols plays a significant role in the establishment of explicit correlation between $PM_{2.5}$ and AOD. In addition, high cloud fraction and relative humidity tend to weaken the correlation, regardless of geographical location. Therefore, the impact of meteorology could be one of the most plausible alternatives in explaining the varying *R* values observed, due to its non-negligible effect on MODIS AOD retrievals. Our findings have implications for $PM_{2.5}$ remote sensing, as long as the aerosol diurnal cycle, along with meteorology, are explicitly considered in the future.

1. Introduction

Aerosols have been extensively suggested to play an important role in climate change on regional and global scales, largely due to their significant but uncertain direct and indirect effects (e.g., Kaufman et al., 2002; Rosenfeld et al., 2008; Li et al., 2011; IPCC, 2013; Wang et al., 2014a; Guo et al., 2016a). In addition, $PM_{2.5}$ (particulate matter with an aerodynamic diameter smaller than 2.5 μm) is believed to be closely associated with a wide range of adverse health effects, including cardiovascular, respiratory diseases, and even premature death (e.g., Al-Saadi et al., 2005; Vidot et al., 2007; Wang et al., 2010; Apte et al., 2015; Schwartz et al., 2015). Therefore, the ability of getting accurate temporal and spatial distribution of ground-based $PM_{2.5}$ becomes an increasingly key prerequisite for the effective reduction and prevention of aerosol pollution (Wang and Christopher, 2003; Lin et al., 2015; Guo et al., 2016b).

Apart from the traditional surface $PM_{2.5}$ monitoring network,

☆ This paper has been recommended for acceptance by Yuan Wang.

* Corresponding author.
** Corresponding author.
E-mail addresses: jpguocams@gmail.com (J. Guo), yzhang@cma.gov.cn (Y. Zhang).

http://dx.doi.org/10.1016/j.envpol.2016.11.043

satellite remote sensing with large spatial coverage and reliable repeated measurements is a very promising approach to monitor the large-scale aerosol loadings and their transport pathways, especially over the remote regions where ground-based observations are sparse (Kaufman et al., 2002; Wang and Christopher, 2003; Engel-Cox et al., 2004; van Donkelaar et al., 2006; Vidot et al., 2007; Wang et al., 2010; Creamean et al., 2013). For instance, the Moderate Resolution Imaging Spectroradiometer (MODIS) onboard the polar orbiting satellites of Terra/Aqua can provide long-term global aerosol optical depth (AOD), a measure of extinction by aerosols in the atmospheric column (Remer et al., 2005). The MODIS AOD data have been widely used to estimate near-surface PM concentration, with accuracy differing greatly by regions (Hauser et al., 2005; Al-Saadi et al., 2005; Gupta et al., 2006; Kumar et al., 2008, 2011; Gupta and Christopher, 2008; Kim et al., 2013; Li et al., 2015; Lin et al., 2015).

The estimation methods of near-surface $PM_{2.5}$ from space-borne AOD can be classified into two categories: observation- and simulation-based methods (Lin et al., 2015). The observation-based methods largely rely on statistical relationships between AOD and surface-level $PM_{2.5}$ observations, which was initially conducted in the United States by Wang and Christopher (2003), who compared MODIS AOD with seven ground measured $PM_{2.5}$ concentrations in Alabama, United States, in 2002, and found that the correlation coefficient (R) between AOD and $PM_{2.5}$ differed by regions, with a maximum R of 0.90. The correlation analyses based on MODIS AOD and $PM_{2.5}$ measurements were then extended throughout the contiguous United States (Engel-Cox et al., 2004), revealing a relatively moderate correlation ($R \approx 0.4$) between MODIS AOD with daily and hourly mean $PM_{2.5}$ concentration. A similar statistical regression study was performed in Europe as well (Koelemeijer et al., 2006). Recently, more sophisticated methods used to estimate $PM_{2.5}$ from space were developed by taking into account meteorological factors such as cloud cover, wind speed, the mixed layer height, and relative humidity (Gupta et al., 2006; Liu et al., 2009; Wang et al., 2010; Zheng et al., 2015). As a consequence, the correlation coefficient between AOD and $PM_{2.5}$ or PM_{10} improved significantly (e.g., Guo et al., 2009; van Donkelaar et al., 2010; Wang et al., 2010; Li et al., 2015).

As a side effect of fast economic development, China is currently suffering from serious aerosol pollution, which leads to increasing attention paid to this region (Xia et al., 2006; Guo et al., 2009; Song, 2009; Wang et al., 2010, 2014b), and underscores the urgent need for real-time air pollution monitoring. However, few operational remote sensing algorithms have been developed to monitor large-scale surface $PM_{2.5}$ concentrations, despite the recent great advances in sophisticated nonlinear methods for $PM_{2.5}$ estimation from space-borne AOD products like multivariate linear models (Seo et al., 2015), back-propagation artificial neural network (e.g., Wu et al., 2012), and geographically weighted regression (GWR) statistical model (e.g., Song et al., 2014; van Donkelaar et al., 2015). This is in part caused by the inhomogeneous horizontal or vertical distributions (Huang et al., 2015), in addition to the meteorology effect in both ground-level $PM_{2.5}$ and satellite AOD retrievals (Li et al., 2015).

It is still challenging to directly estimate ground-level PM2.5 due to difficulty in making comparison of a pixel-wide AOD value with a point observation of $PM_{2.5}$. Large-scale discrepancy between AOD and $PM_{2.5}$ might mask their smaller-scale correspondences (Hutchison et al., 2008; Kumar, 2010). This will be the case if we intentionally or unintentionally ignore the effect caused by the diurnal variation of aerosols. As we know, the diurnal cycle of $PM_{2.5}$ seems to be quite important due to its great impact on various applications, including radiative forcing computation, aerosol-cloud interaction, as well as public health (Smirnov et al., 2002; Arola et al., 2013; Xu et al., 2016), most of which are limited to studies of aerosol optical properties at local scale (Kuang et al., 2015; Xu et al., 2016). To the best of our knowledge, few studies have taken the diurnal variability of $PM_{2.5}$ into account when attempting to develop methods to estimate $PM_{2.5}$ over large scale from space.

Therefore, the objective of this study is to investigate the diurnal cycle of $PM_{2.5}$ based on long-term large-scale $PM_{2.5}$ observational network across China, in addition to conducting correlation analyses between $PM_{2.5}$ and AOD by considering the potential impact of aerosol diurnal cycle, ground-based cloud fraction (CF) and relative humidity (RH). The paper is organized as follows: descriptions of the MODIS-derived AOD, ground-based $PM_{2.5}$, RH and CF measurements in China are presented in section 2. The results concerning the correlation analysis between AOD and $PM_{2.5}$, and its influential factors are presented in section 3. Section 4 gives the major conclusions.

2. Data and method

2.1. $PM_{2.5}$ observations and their processing

Hourly ground-based $PM_{2.5}$ measurements during the period from January 1, 2013 to December 31, 2015 were obtained from 226 sites, which constitute one indispensible part of the China Atmosphere Watch Network (CAWNET) operated by the China Meteorological Administration (CMA). CAWNET was mainly designed to measure ambient aerosol loadings across China, and most of its sites are located in suburban areas, in sharp contrast to the urban settings of the $PM_{2.5}$ sites which belong to the observational network maintained by the Ministry of Environment Protection of China. The latter network takes continuous $PM_{2.5}$ measurements primarily from the Tapered Element Oscillating Microbalance (TEOM) with an accuracy of ± 5 μg m^{-3} for 10 min-averaged data and ± 1.5 μg m^{-3} for hourly averages. It is well known that $PM_{2.5}$ has to be measured at RH <40% (e.g., Barnaba et al., 2010), and all the $PM_{2.5}$ data have undergone strict quality control according to the criteria described in detail by Guo et al. (2009).

All ground-based $PM_{2.5}$ measurements are recorded in Beijing time (BJT). In order to reflect the real effect of solar radiation on the diurnal variation in $PM_{2.5}$, the time coordinates have to be converted to local solar time (*LST*) using the following formula (Guo et al., 2014):

$$T_{LST} = T_{BJT} - 8 + Lon/15 \quad (1)$$

where T_{LST} denotes the observational time in LST, T_{BJT} denotes the original observational time recorded in BJT, and *Lon* denotes the longitude for a given $PM_{2.5}$ site. To enhance visual interpretation, for a given PM2.5 observation station, each daily 24-h period is divided into four 6-hourly intervals defined as follows: early morning (0000–0600 LST), morning (0600–1200 LST), afternoon (1200–1800 LST), and evening (1800–2400 LST).

The diurnal cycles of $PM_{2.5}$ concentration and frequency are determined on the basis of the daily average distribution of hourly time series for the whole period from January 2011 to December 2015. Following the similar methods proposed for characterizing the diurnal variation of precipitation (Guo et al., 2014), the averaged $PM_{2.5}$ at a particular hour of the day $\overline{PM}_{2.5}(x,y,t)$ is expressed as

$$\overline{PM}_{2.5}(x,y,t) = \sum_{d=1}^{d=day} PM_{2.5}(x,y,t,d) \Big/ day \quad (2)$$

where $PM_{2.5}(x,y,t,d)$ represents the $PM_{2.5}$ concentration at "*t*" o'clock ($t = 1, 2, 3 \ldots, 24$) on the day of "d" for a particular site with coordinates (x, y), and "day" represents the total number of days during the three-year period. As such, 24 mean hourly $PM_{2.5}$ values were obtained, each of which was further examined to identify the hour with a maximum in $PM_{2.5}$ concentration (amplitude) and occurrence frequency (phase) for a given day. In this way, the time series of $PM_{2.5}$ concentration (amplitude) and occurrence frequency can be obtained for each site.

2.2. MODIS AOD

The MODIS level 2 AOD data (version 5.1, with a resolution of 10 km × 10 km) for the period January 2013 to December 2015 were downloaded from the Level 1 and Atmosphere Archive and Distribution System (LAADS, https://ladsweb.nascom.nasa.gov/data/search.html). For simplicity, only MODIS-Aqua AOD data which are retrieved at ~1330 LST are used. The MODIS AOD of this version is retrieved using the dual-channel Dark-Target algorithm, which has improved aerosol optical models for the AOD algorithm over land. The algorithm employs primarily three spectral channels centered at 0.47, 0.66, and 2.1 μm respectively. AOD is derived at 0.47 and 0.66 μm, and interpolated to 0.55 μm in order to make comparison with ground-based sun-photometer derived AOD (Anderson et al., 2012).

Extensive field validation campaigns (Wang et al., 2007; Levy et al., 2010) suggested that the MODIS level 2 AOD product has an accuracy of $0.05\tau_a \pm 0.15$ (τ_a represents AOD) over land, high enough for further correlation analyses in the following text.

2.3. Collocation between $PM_{2.5}$ concentration and MODIS AOD

Ground-based measurements are point values, while MODIS AOD is reported at a grid box of 10 km × 10 km (nominal). To investigate the relationship between columnar AOD and surface-level $PM_{2.5}$, both measures must be collocated in space and time. To accomplish realistic spatio-temporal collocation of MODIS AOD and ground-level $PM_{2.5}$, we averaged the original MODIS AOD product (10 km × 10 km) over 50 km × 50 km grid box centered at each $PM_{2.5}$ observational site shown in Fig. 1. Furthermore, continuous $PM_{2.5}$ measurements at each site were collocated with the MODIS-Aqua AOD retrievals within ±30 min of its overpass time. In this way, only the data that were spatially collocated and temporally matched at the MODIS overpasses were obtained and used in the following analyses.

To eliminate the potential influence caused by extreme atmospheric pollution, AOD values greater than 2, as well as PM measurements greater than 400 $\mu g\ m^{-3}$, are excluded. At the same time, only the sites with 30 or more valid pairs of satellite/ground observations (Wilks, 2011) were used to perform correlation analyses.

2.4. Ground-based meteorological observations

The meteorological observations considered here contain RH and total cloud cover (TCC), both of which are obtained from surface weather stations. All of these RH and TCC measurements are made simultaneously with $PM_{2.5}$ concentrations at the same 226 $PM_{2.5}$ sites, which provide an ideal testbed and foundation to investigate how meteorological conditions affect the association of ground-level $PM_{2.5}$ with MODIS AOD. Due to the increasingly deteriorating air quality during recent years (Li et al., 2007; Guo et al., 2011), further correlation analyses were focused on three regions of interest (ROIs): the North China Plain (NCP, 36°N - 41°N, 114°E – 119°E), the Yangtze River Delta (YRD, 30°N - 35°N, 117°E – 123.0°E), the Pearl River Delta (PRD, 20.5°N – 25.5°N, 111.5°E – 116.5°E), which respectively correspond to the red rectangles A, B, and C in Fig. 1b.

RH measurements were made at 3-h intervals each day: 0200 LST, 0500 LST, 0800 LST, 1100 LST, 1400 LST, 1700 LST, 2000 LST, and 2300 LST, respectively. Only 1400 LST RH observations were taken to make more genuine temporal collocation with MODIS-Aqua AOD. Table S1 (in the supplementary materials) shows the statistics with respect to the classification criteria of RH in NCP, YRD, and PRD, respectively. In NCP, the RH ranges of 0–24.5%, 4.5%–39.5%, and 39.5%–100% correspond to "Lowest", "Medium", and "Highest" RH conditions, respectively. In YRD, the "Lowest", "Medium", and "Highest" RH conditions are characterized with RH of 0–40.5%, 40.5%–54.5%, 54.5%–100%, respectively. Similar thresholds hold true for PRD, which have 0–45.5%, 45.5%–56.5%, and 56.5%–100%, respectively.

Cloud observations at weather sites operated by CMA include TCC and low cloud cover, both of which are measured by human observers. The observations are made at 1-h intervals at the national climate observation stations, and made at 3-h intervals at national basic weather observation stations (Xia, 2012). The TCC is the fraction of sky covered by clouds, ranging from 0 to 10. The observation with TCC of zero is referred to as clear and that with TCC of ten is referred to as overcast.

To facilitate the elucidation of how the TCC influences the correlation between AOD and $PM_{2.5}$, three TCC categories were defined (Table S2 in the supplementary materials): "Clear sky", "Median cloudy", and "High cloudy", each of which contains an equal number of samples. The thresholds for these three TCC categories large vary by region.

3. Results and discussion

3.1. Spatial distribution of aerosol particles

As shown in Fig. 1a, the most populous regions like Pearl River Delta (PRD), North China Plain (NCP), and Sichuan Basin, which are generally characterized with high industrialization and intense anthropogenic emissions, have AOD values up to 1.2 or larger. Generally, regions with high $PM_{2.5}$ concentrations coincide with high AOD loadings (Fig. 1b), with the exception of southeastern China (e.g., PRD) and northwestern China. For instance, high AOD can be distinctly seen in northwestern China where dust or dust storms prevail, which generally results in high PM_{10} concentrations. But relatively low $PM_{2.5}$ concentration can be seen in this region (Fig. 1b), indicating aerosol particles with a large aerodynamic diameter contribute to these high AOD values. On the whole, MODIS AOD exhibits a similar spatial pattern as $PM_{2.5}$. That is to say, the regions with great AOD typically correspond to those with high $PM_{2.5}$ concentrations.

Fig. S1 (in supplementary materials) shows the spatial distribution of valid MODIS-Aqua AOD samples (in percentage) for each 1° × 1° domain of China for spring (March-April-May), summer (June-July-August), fall (September-October-November), and winter (December-January-February). In terms of seasonal difference of valid MODIS samples, NCP can reach to as low as 20% in winter, in comparison with 60–80% in the other three seasons. PRD has relatively lower valid AOD samples (20–50%) compared to the other areas, depending on the seasons. What's more interesting is that large climatological AOD is found in the PRD region, contrary to the relatively small $PM_{2.5}$ concentration. This is mostly likely due to the persistent high cloud coverage over this region (Wang et al., 2015), since cloud cover often exerts considerable contamination on the AOD, but can hardly affect the ground-based $PM_{2.5}$ measurements. The observed limited valid AOD samples over PRD, therefore, could at least in part account for the observed mismatch between the two quite different metrics for aerosol loadings: AOD

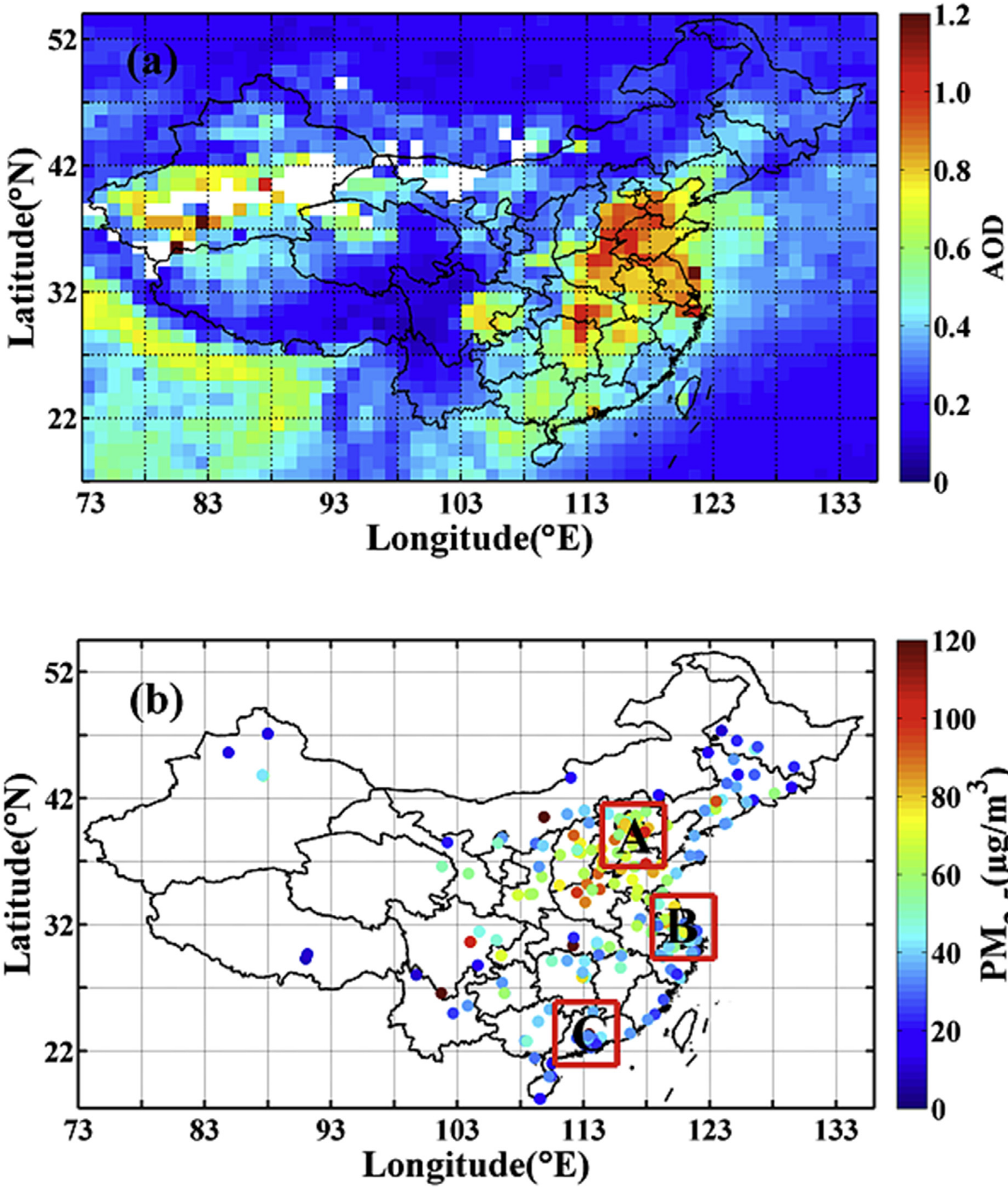

Fig. 1. Spatial distributions of (a) AOD from MODIS onboard Aqua averaged over the period from January 2013 to December 2015, and (b) ground-based $PM_{2.5}$ concentrations (in units of $\mu g\ m^{-3}$) averaged over 1300 LST - 1400 LST during the same period. The following regions of interest (ROIs) are highlighted with red boxes: (A) North China Plain (NCP), (B) Yangtze River Delta (YRD), and (C) Pearl River Delta (PRD). (For interpretation of the references to colour in this figure legend, the reader is referred to the web version of this article.)

versus $PM_{2.5}$.

3.2. *Diurnal variability of $PM_{2.5}$*

Fig. 2 presents the spatial distribution of diurnal phase and amplitude of $PM_{2.5}$ averaged during the period from January 2013 to December 2015 according to maximum mean $PM_{2.5}$ concentration and maximum occurrence frequency of $PM_{2.5}$ peak for each hour within the 24 h. To minimize the impact caused by the recorded time zone (BJT), all hourly $PM_{2.5}$ concentrations are subjected to the conversion procedures based on Eq. (1) in section 2.1. As such, the diurnal cycles of both $PM_{2.5}$ concentration and occurrence frequency can be determined.

Overall, among the 226 $PM_{2.5}$ observational sites, maximum $PM_{2.5}$ concentrations occur in the morning at 107 sites (about 47.3%), followed by 85 sites (37.6%) with peaks in the evening. On the other hand, only 12 sites (5.3%) have the afternoon peak, whereas 22 sites (9.8%) have the early morning peak. The story with

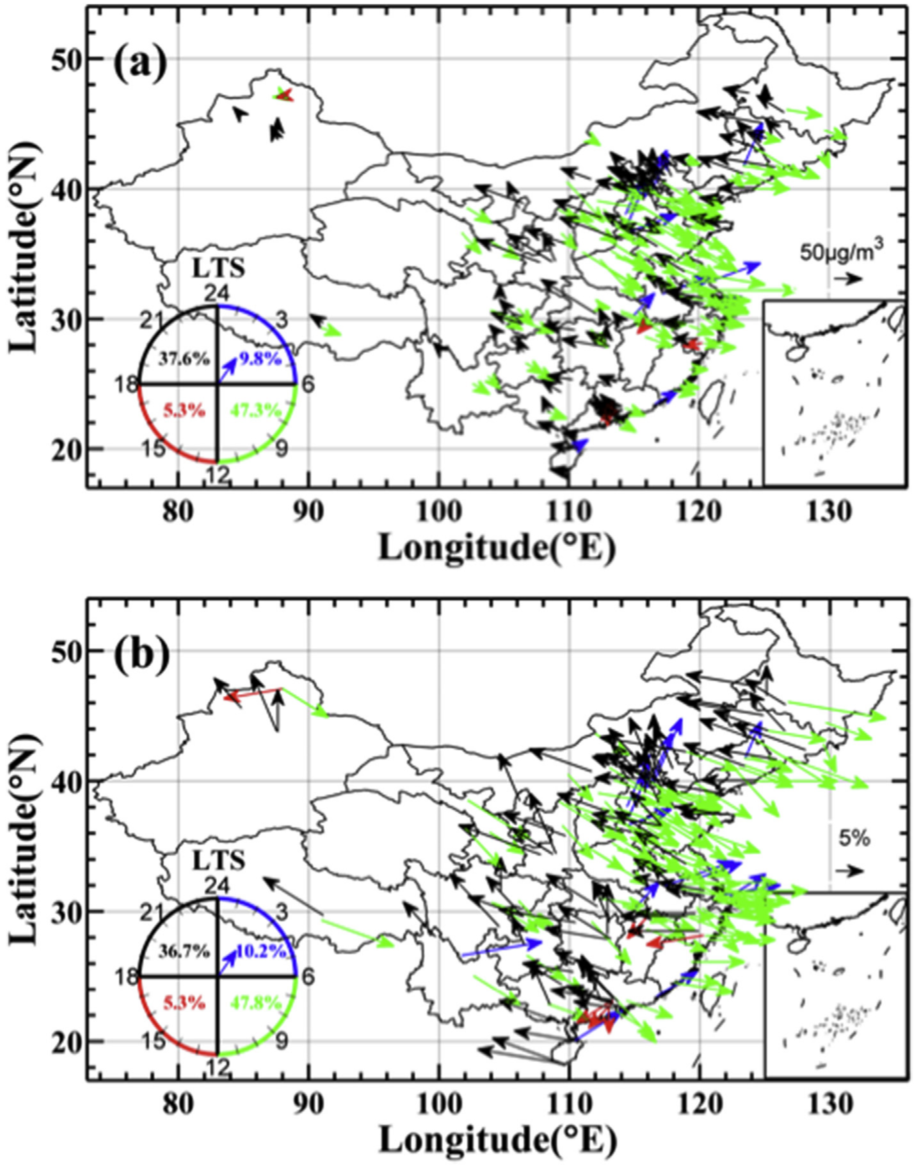

Fig. 2. Diurnal phase and amplitude of $PM_{2.5}$ averaged over the period from January 2013 to December 2015 according to (a) maximum mean $PM_{2.5}$ concentration, and (b) maximum occurring frequency of $PM_{2.5}$ peak for each hour of the 24 h. The direction towards which an arrow points denotes the local solar time (LST) when the maximum occurs (shown on the clock dial in the bottom left corner of each panel) and the arrow length represents magnitudes of $PM_{2.5}$ concentration or frequency. The arrow color denotes varying diurnal phases: blue (0000–0600 LST), green (0600–1200 LST), red (1200–1800 LST) and black (1800–2400 LST). (For interpretation of the references to colour in this figure legend, the reader is referred to the web version of this article.)

respect to the diurnal phase and amplitude of maximum frequency of $PM_{2.5}$ is almost the same (Fig. 2b). In terms of the spatial pattern, the timing of maximum $PM_{2.5}$ concentration agrees well with the diurnal cycle of its occurrence frequency. To be more specific, peak $PM_{2.5}$ generally occurs in the evening in the Pearl River Delta region (YRD in Fig. 1b) of southern China, where sporadic sites witness an afternoon or evening $PM_{2.5}$ maximum (Fig. 2a), with magnitude generally lower than 50 $\mu g\ m^{-3}$. By comparison, both morning and evening $PM_{2.5}$ peaks contribute almost equally to the diurnal cycle in the North China Plain region (NCP in Fig. 1b), with amplitude that is twice or three times that over southern China, indicative of the severe air pollution in northern China. Interestingly, observational sites in northeastern China also have large diurnal amplitude and the maximum $PM_{2.5}$ tends to occur in the morning and evening. This further bears out the AOD and $PM_{2.5}$ pattern observed in Fig. 1. Besides, morning $PM_{2.5}$ peak dominates the Yangze River Delta region (YRD in Fig. 1b), with amplitude lying between those of NCP and PRD.

3.3. The spatio-temporal variability of correlation between $PM_{2.5}$ and AOD

In order to better characterize the regional features, correlation analyses between $PM_{2.5}$ and AOD have been performed over all the sites shown in Fig. 1b, through downscaling to regional scale. Namely, we divided the 226 monitoring sites into 23 sub-domains, each of which has a domain size of $5^\circ \times 5^\circ$. The scatter plots of ground-based in-situ $PM_{2.5}$ against AOD, as well as their concomitant correlation coefficients (R) in these 23 sub-domains are shown in Fig. 3. The *R* values range from 0.17 to 0.57, exhibiting large regional variability, which is in good agreement with the results found in United States (Li et al., 2015). In particular, *R* values in

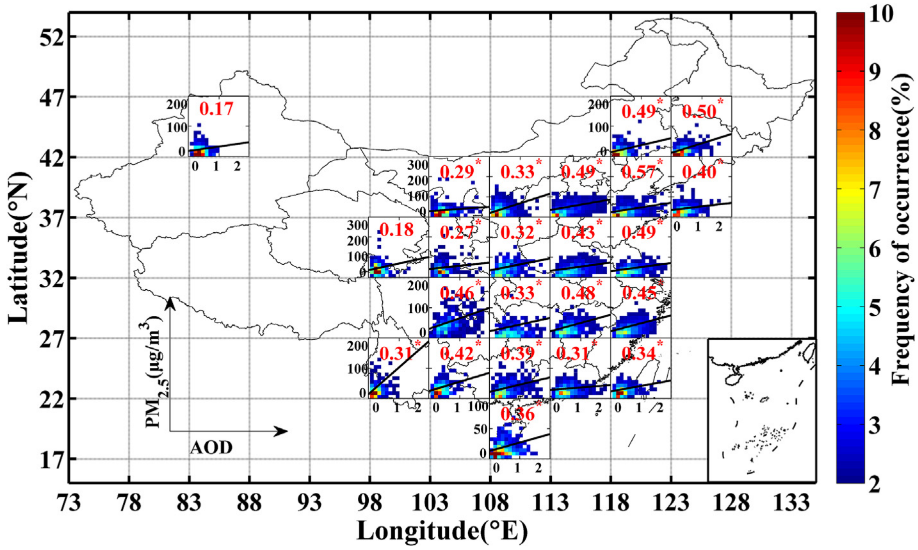

Fig. 3. Scatter plots of ground-based $PM_{2.5}$ against coincident MODIS-Aqua AOD for each 5° × 5° subdomain with enough $PM_{2.5}$ observations. The color shading represents frequency of occurrence for each bin of 0.1 AOD × 10 μg m^{-3} $PM_{2.5}$. The regression line and its corresponding correlation coefficients between $PM_{2.5}$ and AOD are given in each subplot as black lines and red numbers, respectively. Note that the asterisk in the superscript attached to red numbers (R) means the regression is statistically significant ($p < 0.05$). (For interpretation of the references to colour in this figure legend, the reader is referred to the web version of this article.)

eastern China on average are higher than those in western China, where most of the domains have arid conditions and high surface albedos, thereby leading to highly uncertain AOD retrievals (Remer et al., 2005). This in turn results in large biases for the correlation analysis between $PM_{2.5}$ and AOD. A close-up look at sample density distributions (shaded color in Fig. 3) suggests that AOD values for most of the data-pairs are limited to less than 0.5, and $PM_{2.5}$ limited to less than 50 μg m^{-3}. This further supports the results shown in Fig. 3a.

Fig. 4 compares the correlation coefficients for the regression analyses between $PM_{2.5}$ concentration and AOD in different seasons throughout China. In terms of the seasonal variability of R, there exists a large spatial discrepancy. In particular, *R* values generally range from 0.5 to 0.8 in Northeast China, NCP, and YRD, indicating that AOD is a good indicator of $PM_{2.5}$ pollution levels in these regions. In addition, we notice that R is relatively low in areas with complex topography, such as southwestern China, which agrees with previous results (e.g., Xie et al., 2015). Also, the correlation coefficients in coastal areas can not be as high, which may be related to the difficulties in dealing with complex aerosol types and underlying surface albedo in the AOD inversion algorithm applied to the coastal areas (van Donkelaar et al., 2006; Anderson et al., 2012).

As shown in Table 1, the annually averaged R over NCP can be as high as 0.54, gradually reduced to 0.46 over YRD and then dropping to as low as 0.37 over PRD, indicating *R* values exhibit spatial dependence to some degree. Meanwhile, the MODIS-derived AOD is found to be most closely associated with the ground-based $PM_{2.5}$ pollution level in spring over NCP with the highest *R* value (0.71). In contrast, the highest R (0.55) occurs in winter over YRD, whereas it occurs in fall over PRD with $R = 0.45$.

3.4. Impact of various spatio-temporal average schemes on the correlation between AOD and $PM_{2.5}$

As previously demonstrated in section 3.2, significant diurnal variation in $PM_{2.5}$ has been widely observed. Here we selected three ROIs (NCP, PRD, and YRD) to further determine whether or not the diurnal cycle of $PM_{2.5}$ will influence the correlation analyses between AOD and $PM_{2.5}$, and how. As illustrated in Fig. 5, the occurrence time with the maximum averaged $PM_{2.5}$ values is quite different, depending on geographical locations. The $PM_{2.5}$ (112 μg m^{-3}) peaks at midnight over NCP, as compared with the evening peak (67 μg m^{-3}) over YRD, and the morning peak (36 μg m^{-3}) over PRD. In contrast, the lowest $PM_{2.5}$ values occur uniformly at 1400–1600 LST, irrespective of NCP, YRD, and PRD. This could be due to the increased incident solar radiation, which has been suggested to be closely linked to enhanced turbulence and buoyancy and elevated boundary layer height (Guo et al., 2016c).

It is intriguing to note that all the correlation coefficients (individual 1-h mean $PM_{2.5}$ versus MODIS-Aqua AOD) over three ROIs peaks at 1330 LST, then decreases slowly as the $PM_{2.5}$ observational time moves further away from 1330 LST. Therefore, except for the perennially high $PM_{2.5}$ values over NCP which deserves more attention, the impact of $PM_{2.5}$ diurnal variability on the remote sensing of ground-based $PM_{2.5}$ should be considered seriously.

Table 2 shows the results concerning correlation analyses between $PM_{2.5}$ and AOD using different temporal averaging schemes of $PM_{2.5}$ centered over MODIS-Aqua observational time (about 1330 LST). The $PM_{2.5}$ concentrations were averaged over 1300 to 1400, 1200 to 1500, 1100 to 1600, and 0000 to 2400 LST and then compared with the corresponding MODIS-Aqua AOD values. Even though the magnitudes differ greatly, *R* values are typically reduced from north to south, despite various temporal averaging schemes. More importantly, the more closer the MODIS-Aqua overpass time to the time $PM_{2.5}$ was taken, the larger the *R* values are. That is to say, the scheme with 3-h, 5-h, and 24-h time windows will result in large biases in constructing realistic regression equations, compared with the 1-h time window. This indicates that the large biases in part reflect the abovementioned temporal mismatch, and more careful attention should be paid to the temporal mismatch between AOD and $PM_{2.5}$, especially for the temporal averaging scheme for hourly $PM_{2.5}$ observations.

In the meanwhile, we have performed sensitive analyses over NCP, YRD, and PRD regarding the impact of MODIS AOD averaging scheme on the changes in correlation between ground-based $PM_{2.5}$ and collocated MODIS AOD, which corresponds to a spatial resolution of 10 km × 10 km, 30 km × 30 km, 50 km × 50 km,

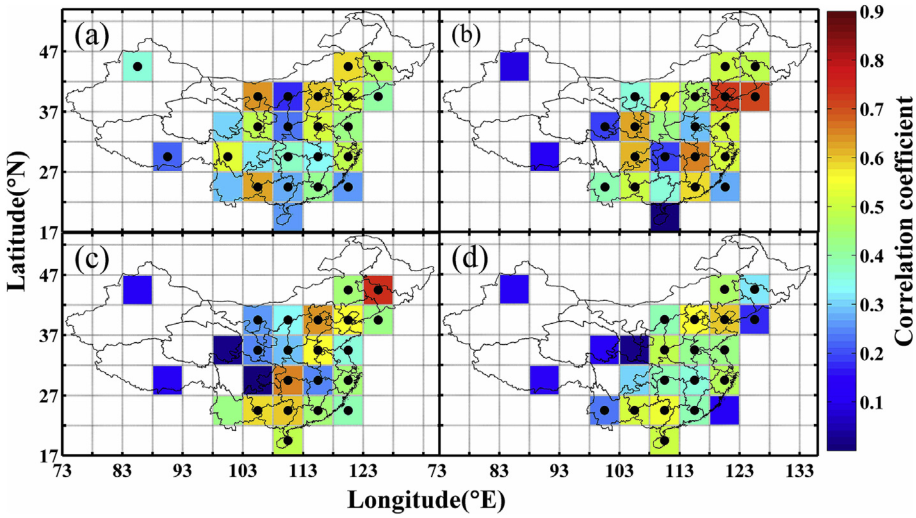

Fig. 4. The spatial distribution of correlation coefficients between ground-based $PM_{2.5}$ and MODIS-Aqua AOD for each 5° × 5° subdomain in (a) spring, (b) summer, (c) fall, and (d) winter over China. The $PM_{2.5}$ measurements made during 1300–1400 BJT were averaged, while the MODIS AOD data were obtained directly from the pixel centered at the corresponding $PM_{2.5}$ observational site during the period of January 2013 to December 2015. The black dots mark grid points where the correlation exceeds 95% significance level ($p < 0.05$) according to the F test.

Table 1
Statistics concerning the correlation coefficients between ground-based seasonally and annually averaged $PM_{2.5}$ concentration and AOD from MODIS onboard Aqua over NCP, YRD, and PRD, during the period of 2013 throughout 2015. Note that the p value is calculated according to F test of the linear regression.

ROI		Spring	Summer	Fall	Winter	Annual
NCP	R	0.71	0.50	0.55	0.59	0.54
	p value	<0.05	<0.05	<0.05	<0.05	<0.05
	# of samples	1657	1680	1008	448	4793
YRD	R	0.36	0.43	0.35	0.55	0.46
	p value	<0.05	<0.05	<0.05	<0.05	<0.05
	# of samples	2043	1506	1368	820	5737
PRD	R	0.36	0.43	0.45	0.38	0.37
	p value	0.12	<0.05	<0.05	<0.05	<0.05
	# of samples	362	452	621	441	1876

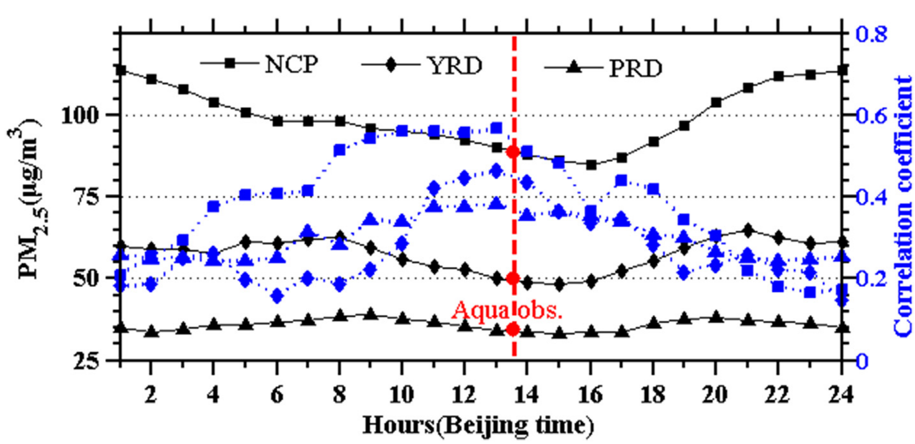

Fig. 5. Diurnal variation of $PM_{2.5}$ concentration (in black curves) and the correlation coefficients (in red curves) between hourly averaged $PM_{2.5}$ concentration and MODIS-Aqua AOD over the domains of NCP (in solid squares), YRD (in solid diamonds), and PRD (in solid triangles) during the period of January 1, 2013 to December 31, 2015. The vertical red dashed line denotes the approximate time when Aqua overpasses the $PM_{2.5}$ observational site. (For interpretation of the references to colour in this figure legend, the reader is referred to the web version of this article.)

respectively. As shown in both Table S3 and Figure S2 in the supplementary material, R values decreases with the size of grid box for averaging the original level 2 MODIS AOD (10 km) when matching AOD and coincident $PM_{2.5}$. This holds true over NCP, YRD, and PRD. Therefore, the correlation between $PM_{2.5}$ and AOD, to some extent, depends on spatial average scheme of MODIS AOD.

3.5. The potential impact of meteorology

Hygroscopic growth of aerosol particles was found to be

Table 2
Summary for the correlation coefficients between 1-h, 3-h, 5-h and 24-h averaged ground-based $PM_{2.5}$ concentration and AOD retrieved from the MODIS onboard Aqua over NCP, YRD, and PRD during the period of 2013 throughout 2015. Note that p value is calculated according to F test to the linear regression.

ROI		1300 - 1400 LST	1200 - 1500 LST	1100 - 1600 LST	0000 - 2400 LST
NCP	R	0.54	0.49	0.50	0.42
	p value	<0.05	<0.05	<0.05	<0.05
	# of samples	4793	5916	6261	6691
YRD	R	0.46	0.41	0.43	0.40
	p value	<0.05	<0.05	<0.05	<0.05
	# of samples	5737	6870	6990	7162
PRD	R	0.37	0.35	0.36	0.34
	p value	<0.05	<0.05	<0.05	<0.05
	# of samples	1876	2108	2149	2235

ubiquitous, which inevitably leads to uncertainties to varying degree in retrieving of AOD from satellite observations (e.g., Remer et al., 2005; Guo et al., 2009). In addition, cloud contamination often induces uncertain or artifact retrievals of satellite- or ground-based AOD (Jeong and Li, 2010; Määttä et al., 2014; Ford and Heald, 2016). Therefore, the effect of RH and cloud fraction on the correlation between $PM_{2.5}$ and AOD merits further detailed and explicit analyses in certain ROIs when $PM_{2.5}$ concentrations are to be estimated from satellite-based AOD (e.g., MODIS-derived AOD).

Fig. S3 (in the supplementary materials) presents the histograms of RH over NCP, YRD, and PRD averaged over the period from 1300 to 1400 LST, matching well with the MODIS-Aqua overpass time. The lowest and highest 30% quantiles of RHs are marked with red dashed lines in each subplot. More details on the criteria have been given for the determination of largest RH and smallest RH conditions. PRD is the most humid region, which is in sharp contrast to the driest NCP. Can this discrepancy in RH have any impact on the regional correlation coefficients derived from the regression analyses of $PM_{2.5}$ against AOD?.

Fig. 6 shows the scatter plots of ground-based $PM_{2.5}$ (averaged over 1300 to 1400 LST) versus the collocated MODIS AOD under different levels of RH over NCP, YRD, and PRD. Overall, regardless of the geographical discrepancy, R exhibits a decreasing trend as the ambient atmosphere becomes more humid. For instance, *R* over NCP is reduced by 30% (from 0.62 to 0.44), as compared with a magnitude of reduction of 37.5% (42.2%) over YRD (PRD). Also, we also notice a distinct southward decrease in R. In other words, the smallest *R* can be seen over PRD (southernmost ROI) for all RH conditions, in sharp contrast to the largest R over NCP (northernmost ROI) and median R over YRD (central ROI). This signifies that RH exerts a significant influence on the correlation between $PM_{2.5}$ and AOD, and cannot be ignored, despite the existing differences in *R* values.

The effect of cloud fraction on correlation analyses between AOD and $PM_{2.5}$ is investigated by separating the matched samples into three equal-sample bins (Table S2). As shown in Fig. 7, R tends to become much higher when all samples are taken under clear sky conditions over NCP, YRD, and PRD, as compared with that under high cloudy conditions. The well-known cloud-induced artificial AOD due to aerosol humidification near clouds (e.g., Twohy et al., 2009), and light scattering from the side of clouds (e.g., Koren et al., 2007; Várnai and Marshak, 2009), generally result in large uncertainties in MODIS AOD retrievals, thereby leading to a deteriorated association of MODIS AOD with ground-based $PM_{2.5}$. Therefore, the confounding meteorological factors like cloud fraction and RH, if any, will make the direct retrieval of $PM_{2.5}$ from MODIS AOD almost impossible due to its adverse impact on R.

4. Concluding remarks

In this study, three years (2013–2015) of ground-based $PM_{2.5}$ data across China were spatio-temporally collocated with MODIS-Aqua AOD data, combined with surface-observed cloud and humidity data to perform explicit correlation analyses.

The diurnal cycles of mass concentration and occurrence frequency of $PM_{2.5}$ are investigated across China. Roughly speaking, one half sites, among the 226 sites, have the maximum $PM_{2.5}$ concentration in the morning, in sharp contrast to the least frequent occurrence (about 5%) in the afternoon, which is most likely due to strong solar radiation received at the surface in the afternoon, thereby leading to the rapid diffusion of aerosol particles and lower mass concentration. Interestingly, the occurrence frequency of $PM_{2.5}$ has almost the same diurnal cycles, as well as its spatial pattern. In particular, $PM_{2.5}$ tends to peak equally in the morning and evening in NCP with amplitudes twice or three times that in PRD. The morning $PM_{2.5}$ peak dominates YRD with amplitudes lying between those of NCP and PRD.

The correlation between surface level $PM_{2.5}$ and MODIS varies greatly in China, both spatially and temporally, which is in good agreement with the previous results. In particular, correlation in eastern China is on average stronger than those in other domains. In terms of the seasonal variability of R, there still exists large spatial discrepancy. MODIS AOD can better represent the surface $PM_{2.5}$ in spring over NCP with the largest R value (0.71). By comparison, maximum correlation ($R = 0.55$) occurs in winter over YRD, whereas it occurs in fall over PRD with $R = 0.45$.

As far as the impact of aerosol diurnal variation on the correlation was concerned, we found that the schemes with 3-h, 5-h, and 24-h time windows have larger biases in constructing realistic regression equations, in comparison with the scheme using 1-h time window. This suggests that the large biases at least partly reflect the above-mentioned temporal mismatch. The impact of meteorology becomes one of the most plausible alternatives that can explain the relatively low *R* values observed in most sites of China, due to its non-negligible effect on MODIS AOD retrievals. The results have great implications for future $PM_{2.5}$ remote sensing from space.

Nevertheless, accurate estimation of the association of $PM_{2.5}$ with AOD remains extremely challenging because both $PM_{2.5}$ and AOD co-vary with meteorological conditions, including cloud fraction and relative humidity. Even though the effect of meteorological factors like CF and RH has been elucidated, the boundary layer height along with vertical structure of aerosols, among others, have been sufficiently recognized to be key to modulating the statistical relationship between $PM_{2.5}$ and AOD. Therefore, more work should be warranted in this regard. Furthermore, the aerosol types with differing light absorbing and scattering properties may affect the correlation analysis results to some extent, which merits more attention in the future.

Acknowledgements

This work was supported by the key technology of integration of

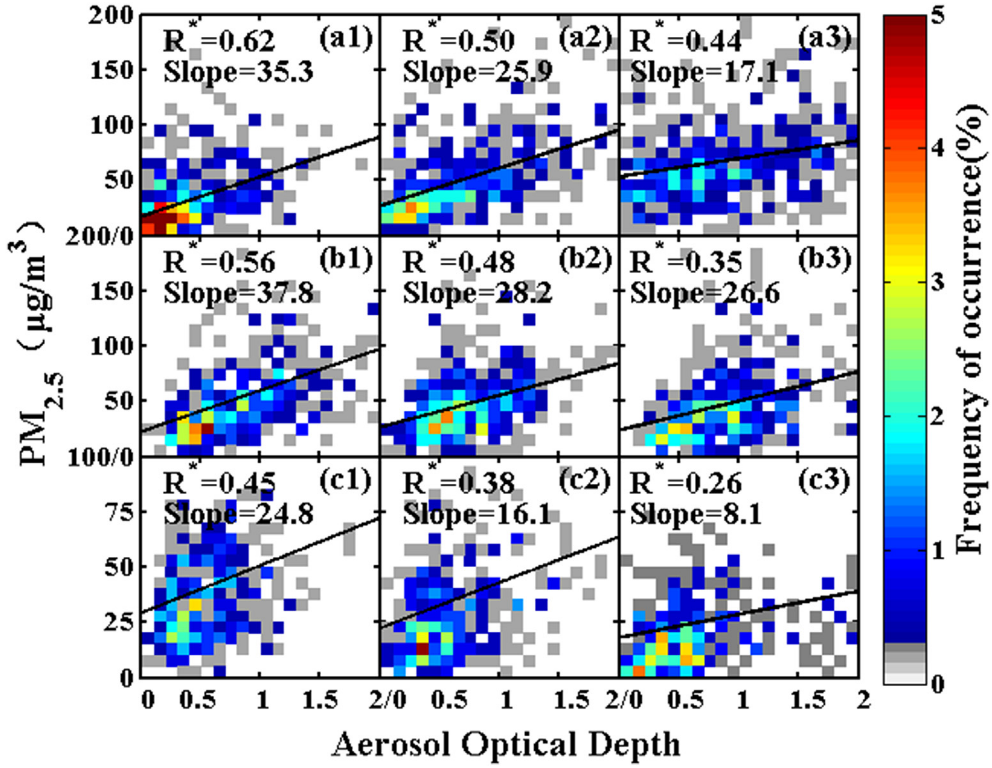

Fig. 6. Joint probability density of AOD vs. $PM_{2.5}$ for low (left column), middle (middle column) and high RH bins (right column) as defined in Table S1 in NCP (top panels), YRD (middle panels), PRD (bottom panels). The correlation coefficient and slope are given in each subplot as well. Note that the bin size of AOD and $PM_{2.5}$ are 0.1 and 10 μg m^{-3} respectively in NCP and YRD, as compared with the bin size of 0.1 and 5 μg m^{-3} in PRD. The color shading denotes the frequency of occurrence for each bin of $PM_{2.5}$-AOD data pairs. The black lines denote least squares fitting lines. Note that the asterisk in superscript attached to *R* value refers to that the regression is statistically significant (p < 0.05).

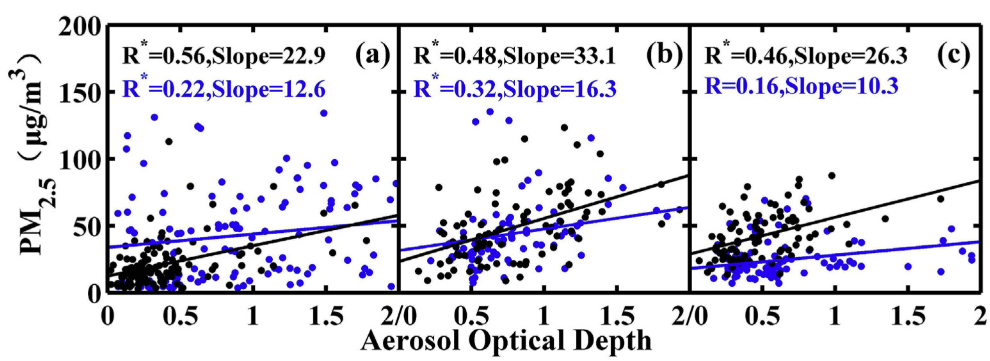

Fig. 7. $PM_{2.5}$ concentrations plotted against MODIS-Aqua AOD under low (in black) and high (in blue) cloud cover conditions over domains of (a) NCP, (b) YRD, and (c) PRD during the period from January 1, 2013 and December 31, 2015. Note that the asterisk in the superscript attached to R value refers to that the regression is statistically significant (p < 0.05). (For interpretation of the references to colour in this figure legend, the reader is referred to the web version of this article.)

meteorological and application projects of CMA under grant CMAGJ2015Z16, the Ministry of Science and Technology of China under Grants 2015DFA20870 and 2014BAC16B01, Natural Science Foundation of China under Grants 91544217 and 41471301, and Chinese Academy of Meteorological Sciences under Grant 2014R18. The $PM_{2.5}$, cloud fraction, RH data used in this paper were acquired from China Meteorological Administration. The MODIS AOD data were acquired from NASA website of https://ladsweb.nascom.nasa.gov/data/search.html. The authors appreciate very much all the data sources. Last but not least, we are grateful to the editor and anonymous reviewers for their constructive comments, which help significantly improve the quality of this manuscript.

Appendix A. Supplementary data

Supplementary data related to this article can be found at http://dx.doi.org/10.1016/j.envpol.2016.11.043.

References

Al-Saadi, J., Szykman, J., Pierce, R.B., Kittaka, C., Neil, D., Chu, D.A., Remer, L., Gumley, L., Prins, E., Weinstock, L., MacDonald, C., Wayland, R., Dimmick, F., Fishman, J., 2005. Improving national air quality forecasts with satellite aerosol observations. Bull. Am. Meteorological Soc. 86, 1249–1261. http://dx.doi.org/10.1175/BAMS-86-9-1249.

Anderson, C., Wang, J., Zeng, J., Petrenko, M., Leptoukh, G.G., Ichoku, C., 2012.

Accuracy assessment of Aqua-MODIS aerosol optical depth over coastal regions: importance of quality flag and sea surface wind speed. Atmos. Meas. Tech. Discuss. 5, 5205–5243. http://dx.doi.org/10.5194/amtd-5-5205-2012.
Apte, J.S., Marshall, J.D., Cohen, A.J., Brauer, M., 2015. Addressing global mortality from ambient $PM_{2.5}$. Environ. Sci. Technol. 49 (13), 8057–8066. http://dx.doi.org/10.1021/acs.est.5b01236.
Arola, A., Eck, T.F., Huttunen, J., Lehtinen, K.E.J., Lindfors, A.V., Myhre, G., Smirnov, A., Tripathi, S.N., Yu, H., 2013. Influence of observed diurnal cycles of aerosol optical depth on aerosol direct radiative effect. Atmos. Chem. Phys. 13, 7895–7901. http://dx.doi.org/10.5194/acp-13-7895-2013.
Barnaba, F., Putaud, J.P., Gruening, C., dell'Acqua, A., Dos Santos, S., 2010. Annual cycle in co-located in situ, total-column, and height-resolved aerosol observations in the Po Valley (Italy): implications for ground-level particulate matter mass concentration estimation from remote sensing. J. Geophys. Res. - Atmos. 115 (D19) http://dx.doi.org/10.1029/2009JD013002.
Creamean, J.M., Suski, K.J., Rosenfeld, D., Cazorla, A., DeMott, P.J., Sullivan, R.C., White, A.B., Ralph, F.M., Minnis, P., Comstock, J.M., Tomlinson, J.M., Prather, K.A., 2013. Dust and biological aerosols from the Sahara and Asia influence precipitation in the western U.S. Science 339 (6127), 1572–1578. http://dx.doi.org/10.1126/science.1227279.
Engel-Cox, J.A., Holloman, C.H., Coutant, B.W., Hoff, R.M., 2004. Qualitative and quantitative evaluation of MODIS satellite sensor data for regional and urban scale air quality. Atmos. Environ. 38, 2495–2509. http://dx.doi.org/10.1016/j.atmosenv.2004.01.039.
Ford, B., Heald, C.L., 2016. Exploring the uncertainty associated with satellite-based estimates of premature mortality due to exposure to fine particulate matter. Atmos. Chem. Phys. 16, 3499–3523. http://dx.doi.org/10.5194/acp-16-3499-2016.
Guo, J.-P., Zhang, X.-Y., Che, H.-Z., Gong, S.-L., An, X., Cao, C.-X., Guang, J., Zhang, H., Wang, Y.-Q., Zhang, X.-C., Xue, M., Li, X.-W., 2009. Correlation between PM concentrations and aerosol optical depth in eastern China. Atmos. Environ. 43, 5876–5886. http://dx.doi.org/10.1016/j.atmosenv.2009.08.026.
Guo, J.P., Zhang, X.Y., Wu, Y.R., Che, Laba, H.Z., Li, X., 2011. Spatio-temporal variation trends of satellite-based aerosol optical depth in China during 1980-2008. Atmos. Environ. 45 (37), 6802–6811.
Guo, J.P., Zhai, P., Wu, L., Cribb, M., Li, Z., Ma, Z., Wang, F., Chu, D., Wang, P., Zhang, J., 2014. Diurnal variation and the influential factors of precipitation from surface and satellite Measurements in Tibet. Int. J. Climatol. 34 (9), 2940–2956. http://dx.doi.org/10.1002/joc.3886.
Guo, J., Deng, M., Lee, S.S., Wang, F., Li, Z., Zhai, P., Liu, H., Lv, W., Yao, W., Li, X., 2016a. Delaying precipitation and lightning by air pollution over the Pearl River Delta. Part I: observational analyses. J. Geophys. Res. Atmos. 121, 6472–6488. http://dx.doi.org/10.1002/2015JD023257.
Guo, J.P., He, J., Liu, H.L., Miao, Y.C., Liu, H., Zhai, P.M., 2016b. Impact of various emission control schemes on air quality using WRF-Chem during APEC China 2014. Atmos. Environ. 140, 311–319. http://dx.doi.org/10.1016/j.atmosenv.2016.05.046.
Guo, J., Miao, Y., Zhang, Y., Liu, H., Li, Z., Zhang, W., He, J., Lou, M., Yan, Y., Bian, L., Zhai, P., 2016c. The climatology of planetary boundary layer height in China derived from radiosonde and reanalysis data. Atmos. Chem. Phys. 16, 13309–13319. http://dx.doi.org/10.5194/acp- 16-13309-2016, 2016.
Gupta, P., Christopher, S.A., 2008. An evaluation of Terra-MODIS sampling for monthly and annual particulate matter air quality assessment over the Southeastern United States. Atmos. Environ. 42, 6465–6471. http://dx.doi.org/10.1016/j.atmosenv.2008.04.044.
Gupta, P., Christopher, S.A., Wang, J., Gehrig, R., Lee, Y., Kumar, N., 2006. Satellite remote sensing of particulate matter and air quality assessment over global cities. Atmos. Environ. 40, 5880–5892. http://dx.doi.org/10.1016/j.atmosenv.2006.03.016.
Hauser, A., Oesch, D., Foppa, N., 2005. Aerosol optical depth over land: comparing AERONET, AVHRR and MODIS. Geophys. Res. Lett. 32 (17) http://dx.doi.org/10.1029/2005GL023579.
Huang, J., Guo, J., Wang, F., Liu, Z., Jeong, M.-J., Yu, H., Zhang, Z., 2015. CALIPSO inferred most probable heights of global dust and smoke layers. J. Geophys. Research-Atmosphere 120 (10), 5085–5100. http://dx.doi.org/10.1002/2014JD022898.
Hutchison, K.D., Faruqui, S.J., Smith, S., 2008. Improving correlations between MODIS aerosol optical thickness and ground-based PM2.5 observations through 3D spatial analyses. Atmos. Environ. 42, 530–543. http://dx.doi.org/10.1016/j.atmosenv.2007.09.050.
IPCC, 2013. Climate change 2013: the physical science basis. In: Stocker, T.F., Qin, D., Plattner, G.-K., Tignor, M., Allen, S.K., Boschung, J., Nauels, A., Xia, Y., Bex, V., Midgley, P.M. (Eds.), Contribution of Working Group I to the Fifth Assessment Report of the Intergovernmental Panel on Climate Change. Cambridge University Press, Cambridge, United Kingdom and New York, NY, USA, p. 1535.
Jeong, M.-J., Li, Z., 2010. Separating real and apparent effects of cloud, humidity, and dynamics on aerosol optical thickness near cloud edges. J. Geophys. Res. Atmos. 115, D00K32. http://dx.doi.org/10.1029/2009JD013547.
Kaufman, Y.J., Tanré, D., Boucher, O., 2002. A satellite view of aerosols in the climate system. Nature 114 (13). http://dx.doi.org/10.1038/nature01091.
Kim, M., Zhang, X., Holt, J.B., Liu, Y., 2013. Spatio-temporal variations in the associations between hourly PM and aerosol optical depth (AOD) from MODIS sensors on Terra and Aqua. Health 5 (10A2), 8–13. http://dx.doi.org/10.4236/health.2013.510A2002.
Koelemeijer, R., Homan, C., Matthijsen, J., 2006. Comparison of spatial and temporal variations of aerosol optical thickness and particulate matter over Europe. Atmos. Environ. 40, 5304–5315.
Koren, I., Remer, L.A., Kaufman, Y.J., Rudich, Y., Martins, J.V., 2007. On the twilight zone between clouds and aerosols. Geophys. Res. Lett. 34, L08805. http://dx.doi.org/10.1029/2007GL029253.
Kuang, Y., Zhao, C.S., Tao, J.C., Ma, N., 2015. Diurnal variations of aerosol optical properties in the North China Plain and their influences on the estimates of direct aerosol radiative effect. Atmos. Atmos. Chem. Phys. 15, 5761–5772. http://dx.doi.org/10.5194/acp-15-5761-2015.
Kumar, N., 2010. What can affect AOD-PM2.5 association. Environ. Health Perspect. 118 (3), A109–A110. http://dx.doi.org/10.1289/ehp.0901732.
Kumar, N., Chu, A., Foster, A., 2008. Remote sensing of ambient particles in Delhi and its environs: estimation and validation. Int. J. Remote Sens. 29, 3383–3405. http://dx.doi.org/10.1080/01431160701474545.
Kumar, N., Chu, A.D., Foster, A.D., Peters, T., Willis, R., 2011. Satellite remote sensing for developing time and space resolved estimates of ambient particulate in Cleveland, OH. Aerosol Sci. Technol. 45, 1090–1108. http://dx.doi.org/10.1080/02786826.2011.581256.
Levy, R.C., Remer, L.A., Kleidman, R.G., Mattoo, S., Ichoku, C., Kahn, R., Eck, T., 2010. Global evaluation of the Collection 5 MODIS dark-target aerosol products over land. Atmos. Chem. Phys. 10 (21), 10399–10420.
Li, Z., et al., 2007. Preface to special section on east asian study of tropospheric aerosols: an international regional experiment (EAST-AIRE). J. Geophys. Res. Atmos. D22S00. http://dx.doi.org/10.1029/2007JD008853.
Li, Z., Niu, F., Fan, J., Liu, Y., Rosenfeld, D., Ding, Y., 2011. Long-term impacts of aerosols on the vertical development of clouds and precipitation. Nat. Geosci. 4, 888–894.
Li, J., Carlson, B.E., Lacis, A.A., 2015. How well do satellite AOD observations represent the spatial and temporal variability of $PM_{2.5}$ concentration for the United States? Atmos. Environ. 102, 260–273. http://dx.doi.org/10.1016/j.atmosenv.2014.12.010.
Lin, C., Li, Y., Yuan, Z., Lau, A.K.H., Li, C., Fung, J.C.H., 2015. Using satellite remote sensing data to estimate the high-resolution distribution of ground-level PM2.5. Remote Sens. Environ. 156, 117–128. http://dx.doi.org/10.1016/j.rse.2014.09.015.
Liu, Y., Paciorek, C.J., Koutrakis, P., 2009. Estimating regional spatial and temporal variability of PM2.5 concentrations using satellite data, meteorology, and land use information. Environ. Health Perspect. 117 (6), 886–892. http://dx.doi.org/10.1289/ehp.0800123.
Määttä, A., Laine, M., Tamminen, J., Veefkind, J.P., 2014. Quantification of uncertainty in aerosol optical thickness retrieval arising from aerosol microphysical model and other sources, applied to Ozone Monitoring Instrument (OMI) measurements. Atmos. Meas. Tech. 7, 1185–1199. http://dx.doi.org/10.5194/amt-7-1185-2014.
Remer, L.A., Kaufman, Y.J., Tanré, D., Mattoo, S., Chu, D.A., Martins, J.V., Li, R.R., Ichoku, C., Levy, R.C., Kleidman, R.G., Eck, T.F., Vermote, E., Holben, B.N., 2005. The MODIS aerosol algorithm, products, and validation. J. Atmos. Sci. 62 (4), 947–973. http://dx.doi.org/10.1175/jas3385.1.
Rosenfeld, D., Lohmann, U., Raga, G.B., O'Dowd, C.D., Kulmala, M., Fuzzi, S., Reissell, A., Andreae, M.O., 2008. Flood or drought: how do aerosols affect precipitation? Science 321, 1309–1313.
Schwartz, J.D., Melly, S.J., Koutrakis, P., Coull, B.A., Kloog, I., Zanobetti, A., Shi, L., 2015. Low-concentration PM2.5 and mortality: estimating acute and chronic effects in a population-based study. Environ. Health Perspect. 124 (1), 46. http://dx.doi.org/10.1289/ehp.1409111.
Seo, S., Kim, J., Lee, H., Jeong, U., Kim, W., Holben, B.N., Kim, S.W., Song, C.H., Lim, J.H., 2015. Estimation of PM10 concentrations over Seoul using multiple empirical models with AERONET and MODIS data collected during the DRAGON-Asia campaign. Atmos. Chem. Phys. 15, 319–334. http://dx.doi.org/10.5194/acp-15-319-2015.
Smirnov, A., Holben, B.N., Eck, T.F., Slutsker, I., Chatenet, B., Pinker, R.T., 2002. Diurnal variability of aerosol optical depth observed at AERONET (Aerosol Robotic Network) sites. Geophys. Res. Lett. 29 (23), 301–304. http://dx.doi.org/10.1029/2002GL016305.
Song, C.-K., 2009. Spatial and seasonal variations of surface PM10 concentration and MODIS aerosol optical depth over China. Asia-Pacific J. Atmos. Sci. 45 (1), 33–43.
Song, W., Jia, H., Huang, J., Zhang, Y., 2014. A satellite-based geographically weighted regression model for regional PM2.5 estimation over the Pearl River Delta region in China. Remote Sens. Environ. 154, 1–7. http://dx.doi.org/10.1016/j.rse.2014.08.008.
Twohy, C.H., Coakley Jr., J.A., Tahnk, W.R., 2009. Effect of changes in relative humidity on aerosol scattering near clouds. J. Geophys. Res. Atmos. 114, D05205. http://dx.doi.org/10.1029/2008JD010991.
van Donkelaar, A., Martin, R.V., Park, R.J., 2006. Estimating ground-level PM2.5 using aerosol optical depth determined from satellite remote sensing. J. Geophys. Res. - Atmos. 111 http://dx.doi.org/10.1029/2005JD006996.
van Donkelaar, A., Martin, R.V., Brauer, M., Kahn, R., Levy, R., Verduzco, C., Villeneuve, P.J., 2010. Global estimates of ambient fine particulate matter concentrations from satellite-based aerosol optical depth: development and application. Environ. Health Perspect. 118, 847–855. http://dx.doi.org/10.1289/ehp.0901623.
van Donkelaar, A., Martin, R.V., Spurr, R.J.D., Burnett, R.T., 2015. High-resolution satellite-derived PM2.5 from optimal estimation and geographically weighted regression over North America. Environ. Sci. Technol. 49 (17), 10482–10491.

http://dx.doi.org/10.1021/acs.est.5b02076.

Várnai, T., Marshak, A., 2009. MODIS observations of enhanced clear sky reflectance near clouds. Geophys. Res. Lett. 36 (6), L06807. http://dx.doi.org/10.1029/2008GL037089.

Vidot, J., Santer, R., Ramon, D., 2007. Atmospheric particulate matter (PM) estimation from SeaWiFS imagery. Remote Sens. Environ. 111, 1–10. http://dx.doi.org/10.1016/j.rse.2007.03.009.

Wang, J., Christopher, S.A., 2003. Intercomparison between satellite-derived aerosol optical thickness and $PM_{2.5}$ mass: implications for air quality studies. Geophys. Res. Lett. 30 (21) http://dx.doi.org/10.1029/2003GL018174.

Wang, L., Xin, J., Wang, Y., Li, Z., Wang, P., Liu, G., Wen, X., 2007. Validation of MODIS aerosol products by CSHNET over China. Chin. Sci. Bull. 52 (12), 1708–1718.

Wang, Z., Chen, L., Tao, J., Zhang, Y., Su, L., 2010. Satellite-based estimation of regional particulate matter (PM) in Beijing using vertical-and-RH correcting method. Remote Sens. Environ. 114, 50–63. http://dx.doi.org/10.1016/j.rse.2009.08.009.

Wang, L., Zhang, N., Liu, Z., Sun, Y., Ji, D., Wang, Y., 2014a. The influence of climate factors, meteorological conditions, and boundary-layer structure on severe haze pollution in the beijing-tianjin-hebei region during january 2013. Adv. Meteorology 2014, 1–14. http://dx.doi.org/10.1155/2014/685971.

Wang, Y., Lee, K.-H., Lin, Y., Levy, M., Zhang, R., 2014b. Distinct effects of anthropogenic aerosols on tropical cyclones. Nat. Clim. Change 4, 368–373.

Wang, F., Guo, J., Zhang, J., Huang, J., Min, M., Chen, T., Liu, H., Deng, M., Li, X., 2015. Multi-sensor quantification of aerosol-induced variability in warm cloud properties over eastern China. Atmos. Environ. 113, 1–9. http://dx.doi.org/10.1016/j.atmosenv.2015.04.063.

Wilks, D.S., 2011. Statistical Methods in the Atmospheric Sciences, vol. 100. Academic press, Waltham, MA.

Wu, Y.R., Guo, J., Zhang, X., Tian, X., Zhang, J., Wang, Y., Duan, J., Li, X., 2012. Synergy of satellite and ground based observations in estimation of particulate matter in eastern China. Sci. Total Environ. 433, 20–30. http://dx.doi.org/10.1016/j.scitotenv.2012.06.033.

Xia, X.A., 2012. Significant decreasing cloud cover during 1954–2005 due to more clear-sky days and less overcast days in China and its relation to aerosol. Ann. Geophys. 30 (3), 573–582.

Xia, X.A., Chen, H.B., Wang, P.C., Zhang, W.X., Goloub, P., Chatenet, B., Eck, T.F., Holben, B.N., 2006. Variation of column-integrated aerosol properties in a Chinese urban region. J. Geophys. Res. - Atmos. 111 http://dx.doi.org/10.1029/2005JD006203.

Xie, Y., Wang, Y., Zhang, K., Dong, W., Lv, B., Bai, Y., 2015. Daily estimation of ground-level PM2.5 concentrations over Beijing using 3 km resolution MODIS AOD. Environ. Sci. Technol. 49, 12280–12288. http://dx.doi.org/10.1021/acs.est.5b01413.

Xu, H., Guo, J.P., Ceamanos, X., Roujean, J.L., Min, M., Carrer, D., 2016. On the influence of the diurnal variations of aerosol content to estimate direct aerosol radiative forcing using MODIS data. Atmos. Environ. 141, 186–196. http://dx.doi.org/10.1016/j.atmosenv.2016.06.067.

Zheng, S., Pozzer, A., Cao, C.X., Lelieveld, J., 2015. Long-term (2001–2012) concentrations of fine particulate matter (PM2.5) and the impact on human health in Beijing, China. Atmos. Chem. Phys. 15, 5715–5725. http://dx.doi.org/10.5194/acp-15-5715-2015.